

Prediction and Synthesis of Strain Tolerant RbCuTe Crystals Based on Rotation of One-Dimensional Nano Ribbons within a Three-Dimensional Inorganic Network

Michael J. DeVries Vermeer,^{†,‡,§} Xiuwen Zhang,^{§,¶} Giancarlo Trimarchi,[‡] Martin D. Donakowski,^{†,||} Peter J. Chupas,[¶] Kenneth R. Poeppelmeier,[†] and Alex Zunger^{*,§}

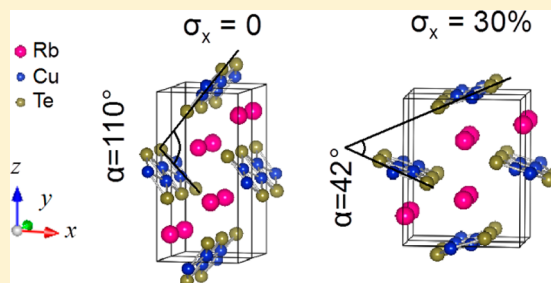
[†]Department of Chemistry and [‡]Department of Physics and Astronomy, Northwestern University, 2145 Sheridan Road, Evanston, Illinois 60208, United States

[§]Renewable and Sustainable Energy Institute, University of Colorado, Boulder, Colorado 80309-0027, United States

[¶]Advanced Photon Source, Argonne National Laboratory, 9700 South Cass Avenue, Argonne, Illinois 60439, United States

Supporting Information

ABSTRACT: A unique possibility for a simple strain tolerant inorganic solid is envisioned whereby a set of isolated, one-dimensional (1D) nano objects are embedded in an elastically soft three-dimensional (3D) atomic matrix thus forming an interdimensional hybrid structure (IDHS). We predict theoretically that the concerted rotation of 1D nano objects could allow such IDHSs to tolerate large strain values with impunity. Searching theoretically among the 1:1:1 ABX compounds of I–I–VI composition, we identified, via first-principles thermodynamic theory, RbCuTe, which is a previously unreported but now predicted-to-be-stable compound in the MgSrSi-type structure, in space group *Pnma*. The predicted structure of RbCuTe consists of ribbons of copper and telluride atoms placed antipolar to one another throughout the lattice with rubidium atoms acting as a matrix. A novel synthetic adaptation utilizing liquid rubidium and vacuum annealing of the mixed elemental reagents in fused silica tubes as well as *in situ* (performed at the Advanced Photon Source) and *ex situ* structure determination confirmed the stability and predicted structure of RbCuTe. First-principles calculations then showed that the application of up to ~30% uniaxial strain on the ground-state structure result in a buildup of internal stress not exceeding 0.5 GPa. The increase in total energy is 15-fold smaller than what is obtained for the same RbCuTe material but in structures having a contiguous set of 3D chemical bonds spanning the entire crystal. Furthermore, electronic structure calculations revealed that the HOMO is a 1D energy band localized on the CuTe ribbons and that the 1D insulating band structure is also resilient to such large strains. This combined theory and experiment study reveals a new type of strain tolerant inorganic material.



1. INTRODUCTION

The ability of certain inorganic crystalline solids to tolerate significant applied pressure or strain without developing dislocations or fractures constitutes an important mechanical attribute. In ordinary three-dimensional (3D) inorganic solids consisting of a contiguous set of chemical bonds, such as silicon or Al₂O₃, applied strain is experienced by the entire set of chemical bonds, a response that makes continuum elasticity an appropriate description for such solids.¹ Strain engineering^{2–4} needed in flexible devices is limited in such 3D solids with continuous bonds by the modest magnitude of strain (e.g., 1% in Si⁵ and 0.1% in Al₂O₃⁶) that can be applied before failure sets in because of the bond breaking. On the other hand, soft insulators and semiconductors needed for flexible devices were sought mostly among highly compressible molecular organic materials^{7–10} formed by isolated one-dimensional (1D) or two-dimensional (2D) units with weak intermolecular interactions. An interesting third category of crystalline packing pertinent to the discussion of strain tolerance is hybrids between the former

two prototypes: isolated zero-dimensional (0D) or 1D molecular units embedded via weak bonds within a 3D framework. For example, metal–organic frameworks^{11–14} are hybrid structures consisting of a soft organic matrix and rigid inorganic cores leading to mechanical flexibility and molecular-level machinelike solid-state dynamics. Here we seek a hybrid inorganic system consisting of an elastically soft atomic 3D lattice (denoted A_{3D}) within which a set of isolated, 1D nano objects (BX)_{1D} are embedded. Unlike the atomic 3D lattice, the latter nano objects possess rigidlike motional degrees of freedom (e.g., they can rotate and tilt) spanning a remarkably wide range. We expect that the concerted rotation of 1D nano ribbons within a soft and adaptable 3D atomic matrix could allow such interdimensional hybrid structures (IDHSs) to tolerate large strain values with impunity.

Received: June 14, 2015

Published: August 14, 2015



Here we explore the possibility of such strain tolerant interdimensional structures within the octet ABX intermetallic compounds. Panels a and b of Figure 1 show the structures of

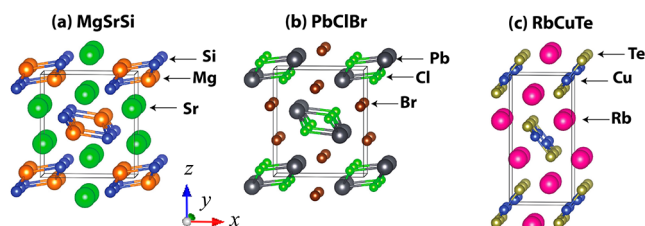


Figure 1. Crystal structures (experimental) of (a) MgSrSi and (b) PbClBr showing unconnected ribbons embedded in a matrix of Sr and Br, respectively. (c) Predicted and subsequently synthesized ground-state structure of RbCuTe discussed in the current work as being strain tolerant, having 1D ribbons of CuTe embedded in a 3D Rb lattice.

the eight-electron II-II-IV compound MgSrSi (part a) and the 18-electron IV-VII-VII compound PbClBr (part b) showing 1D Mg–Si and Pb–Cl ribbons, respectively, embedded in the 3D matrix formed by the third species. There are at least 45 previously explored intermetallic ABX compounds of I-I-VI composition, including, but not limited to, 13 oxides,^{15–19} 13 sulfides,^{20–29} 10 selenides,^{23,30–35} and 9 tellurides.^{23,30,36,37} The structural motif of I-I-VI ABX compounds such as ACuTe ($A = \text{Na}$ or K) has been observed within larger layered A-M-RE-Te₄ structures ($A = \text{Na}$ or K ; $M = \text{Cu}$ or Ag ; $\text{RE} = \text{La}$ or Ce).³⁸ In these structures, the ACuTe motifs can be viewed as distinct layers inserted into the van der Waals gaps of the RE-Te₃ slabs. This separation induced between the RE-Te₃ slabs by the ACuTe layers changes the character of the compound from 3D to a structure 2D in character. Several of the I-I-VI ABX structural motifs, including NaCuTe and KCuTe, have also been synthesized as isolated ABX compounds.³⁰ Reduced dimensionality in structures, notably in chalcogenides, can result in improved radiation detectors, thermoelectrics, and/or nonlinear optics.^{39–41}

Our theoretical interest in the discovery of previously unreported members of known chemical families (“missing compounds”)^{42–46} led us to explore this I-I-VI group in search of interdimensional compounds. We predicted using density functional-based first-principles thermodynamics that the yet-unreported RbCuTe compound would be stable in the orthorhombic *Pnma* MgSrSi-type structure that expresses such an interdimensional architecture, where the Rb atoms organize in a periodic 3D matrix, which includes 1D ribbons, formed by Cu and Te. We then conducted syntheses and avoided often-used binary alkali-chalcogenide reagents^{47,48} (so-called reactive flux⁴⁹), which could not have allowed the desired 1:1:1 reagent stoichiometry, and focused instead on using the reagent that forms the interconnecting A_{3D} lattice. To this end, we use a novel synthetic adaptation utilizing liquid rubidium and vacuum annealing of the mixed elemental reagents in fused silica tubes, finding in crystallographic refinement a set of structural parameters that are close to those predicted (Table 1). Subsequent first-principles calculations discussed below showed that the application to the experimental structure of up to 30% uniaxial strain perpendicular to the nano ribbons results in a buildup of internal stress not exceeding 0.5 GPa and in an increase in total energy of 16 meV/atom that are 15-fold smaller than what is obtained for the same RbCuTe material but in structures having a contiguous set of chemical bonds

Table 1. Crystallographic Parameters for RbCuTe (orthorhombic, *Pnma*, Pearson symbol mP12, $\alpha = \beta = \gamma = 90^\circ$, $Z = 4$) Obtained from Experiment and Local Total-Energy Minimization at the PBEsol, GGA+U, and GGA Levels^a

	single-crystal X-ray	PBEsol (% error)	GGA+U (% error)	GGA (% error)
<i>a</i> (Å)	6.4658(3)	6.526 (0.9%)	6.680 (3.3%)	6.803 (5.2%)
<i>b</i> (Å)	4.3760(2)	4.312 (−1.3%)	4.417 (0.9%)	4.410 (0.8%)
<i>c</i> (Å)	13.3745(6)	13.278 (−0.7%)	13.581 (1.5%)	13.508 (1.0%)
volume (Å ³)	378.4226(6)	374.44 (−1.1%)	400.751 (5.9%)	405.299 (7.1%)

^aThe errors of the theoretical values are given with respect to experimental results.

spanning the entire crystal, such as the cubic half-Heusler form (AgMgAs-type, *F43m*). Electronic structure calculations further show a pseudo-1D band near the valence band maximum (VBM) with the wave function localized on the ribbons, and that the 1D insulating band structure is resilient to such large strains. This new type of inorganic material can be utilized for strain tolerant flexible devices, shape memory matters, and the single-crystal arena of studying mesoscale effects of a periodic array of quantum-confined skeletons that can be fully tuned by external stimuli.

2. PREDICTION OF THE MISSING RbCuTe COMPOUND AND ITS 1D–3D FEATURES

The lowest-energy structure of RbCuTe was previously⁴³ predicted by high-throughput *ab initio* screening of ~40 structure prototypes. Sections I and II of the Supporting Information give the detailed results about the prediction of the lowest-energy crystal structure by structure-type screening (Figures S1 and S2) and of the assessment of its thermodynamic stability (Figure S3) against disproportionation into various combinations of constituents.

The local total-energy minimizations were performed by the conjugate-gradient method setting a tolerance of $\delta E_{\text{scf}} = 10^{-7}$ eV per unit cell for the convergence of the total energy in the self-consistent Kohn–Sham cycle (the “inner loop”) and $\delta E_{\text{ion}} = 10^{-6}$ eV per unit cell for the convergence of the total-energy minimization as a function of the ion positions and lattice vectors. Such a fine tolerance to relaxation is needed because the Born–Oppenheimer surface is very shallow so the determination of minima is sensitive.

The total energies as well as the atomic forces and the stress tensor required for the structure relaxation were tested using three exchange-correlation functionals: (i) PBEsol,⁵⁰ (ii) GGA+U⁵¹ using $U(\text{Cu}) = 5$ eV as used in ref 43, and (iii) GGA.^{52–54} The relaxed lattice constants are listed in Table 1 (Tables S1 and S2 list the atomic coordinates and distances, respectively). The results are all qualitatively similar. PBEsol delivers the best prediction but underestimates *b* and *c*. GGA+U offers the best compromise as it accurately predicts *b* and *c*, with an error that is still close to what is usually considered an acceptable accuracy (i.e., 1–3%). GGA gives the poorest result for this system (5.2% error). Because PBEsol is yet untested for high-order derivatives (as needed in the mapping of energy surfaces as a function of various displacement modes used here), we use in this work GGA+U. Section III of the Supporting Information

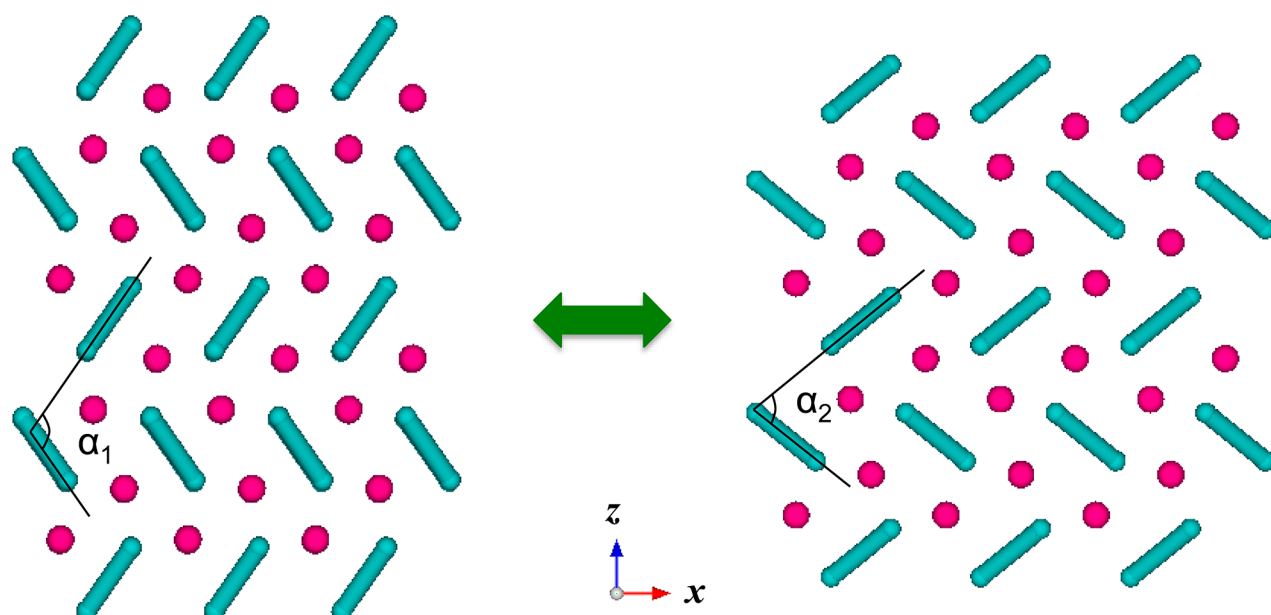


Figure 2. Illustration of the hybrid inorganic structure having rigid 1D nano ribbons (light blue; the ribbon is infinitely long in the y direction) embedded in a 3D matrix (red). Under deformation, the 1D nano ribbons can absorb much of the strain with a minimal increase in energy by using its internal degrees of freedom, i.e., rotating (see angle α_1), whereas the 3D matrix is naturally soft so it does not contribute to a large increase in energy.

provides some comparisons of other results using PBEsol and GGA, reaching qualitatively similar conclusions.

The predicted lowest-energy structure in space group $Pnma$ (Figure 1c and Table 1) consists of ribbons of copper and telluride atoms within the matrix of rubidium atoms. The structural features are precisely those we expect will lead in such IDHSs to strain tolerance; namely, the 3D Rb lattice is elastically soft, whereas the 1D CuTe nano ribbons (with widths of about 1/2 nanometer) can respond to strain by rotations that do not increase the energy much. We next discuss efforts to synthesize this previously unreported compound.

3. SYNTHESIS AND CHARACTERIZATION OF PREDICTED STRUCTURE

3.1. Synthesis. Syntheses of ternary chalcogenide phases often use the binary alkali-chalcogenide compound as one of the reagents,^{47,48} beginning with the first reported use of K_2S as a so-called reactive flux.⁴⁹ It is difficult to achieve the correct stoichiometry for the desired ABX compound, however, because of the inherently complex molar ratios of the reagents and the A_2Q flux. Syntheses were performed via vacuum annealing the elements inside a fused silica ampule. Because of the air-sensitive nature of reagents and products, all preparation and characterization were conducted under a nitrogen atmosphere. In a typical preparation, semisolid rubidium (Alfa Aesar, 99.75%) was first melted in its vessel on a hot plate, and then approximately 3.0 mmol was transferred to the preweighed reaction vessel via pipet.

The rubidium was allowed to cool and solidify before the addition of the other reagents. Copper powder (Sigma-Aldrich, 99.7%) and tellurium powder (Sigma-Aldrich, 99.8%) were added to the reaction vessel in amounts that resulted in a 1:1 molar ratio with the previously added rubidium for each, resulting in an overall molar ratio of reagents of 1:1:1. The reaction vessel was then sealed under vacuum at pressures of $<10^{-4}$ Torr and placed in a furnace for annealing. The reaction

temperature was ramped up to 650 °C at a rate of 5 °C/min, held at 650 °C for 12 h, ramped down to 100 °C at a rate of 0.08 °C/min, and then decreased to room temperature by removal from the furnace.

3.2. In Situ Analyses at the Advanced Photon Source. *In situ* analysis of the reaction was performed on beamline 11-BM at the Advanced Photon Source at Argonne National Laboratory. Diffraction patterns were collected at a wavelength of 0.1430 Å. Diffraction patterns of the reaction were observed with 15 s exposures every 30 s as the vessel containing the three elemental reagents was ramped from 60 to 600 °C at a rate of 5 °C/min. The analysis showed a fast, vigorous reaction occurring within the vessel at approximately 125 °C. On the basis of the products observed upon reaching the final temperature, it was concluded that a significant dwell time at temperature was needed to form and grow single crystals of RbCuTe described next.

3.3. X-ray Analysis, Structural Refinement, and Comparison with Earlier Theoretical Predictions. The reaction vessel was scored and opened under a nitrogen atmosphere. The resulting mass of black crystals was broken in a mortar and pestle, and small crystallites were immersed in inert oil on a microscope slide for sample preparation and transfer to the diffractometer. A metallic, black plate-like single crystal was selected from these crystallites and mounted on a glass fiber for analysis. Crystallographic measurements were taken at 100 K with a Bruker Kappa APEX 2 CCD diffractometer with monochromated Mo $K\alpha$ radiation ($\lambda = 0.71073$ Å) and a crystal–detector distance of 60 mm. The data were integrated with SAINT-V7.23A.⁵⁵ A multiscan absorption correction was applied to the data in the program APEX2 via SADABS.⁵⁶ The structure was then determined using direct methods with XS and refined with the XL refinement package within the Olex2 suite.^{57,58} The results are summarized in Table 1 as well as Tables S1 and S2 of the Supporting Information.

4. STRAIN TOLERANCE: LARGE STRAIN-INDUCED CHANGES IN STRUCTURE LEAD TO A MINIMAL CHANGE IN ENERGY AND STRESS

To illustrate the softness and thus strain tolerance of RbCuTe, we will consider the two types of motions possible for the ribbons, i.e., rotation in x - z plane and shifting along the y direction within the 3D soft matrix of Rb atoms (Figure 2).

4.1. Rotation of the 1D Nano Ribbon Protects the Interdimensional Hybrid System from Stress. The minimum-energy ground-state structure (S_G) of RbCuTe is shown in Figure 3a; it is orthorhombic in space group $Pnma$ with lattice constants listed in Table 1. It consists of a 3D

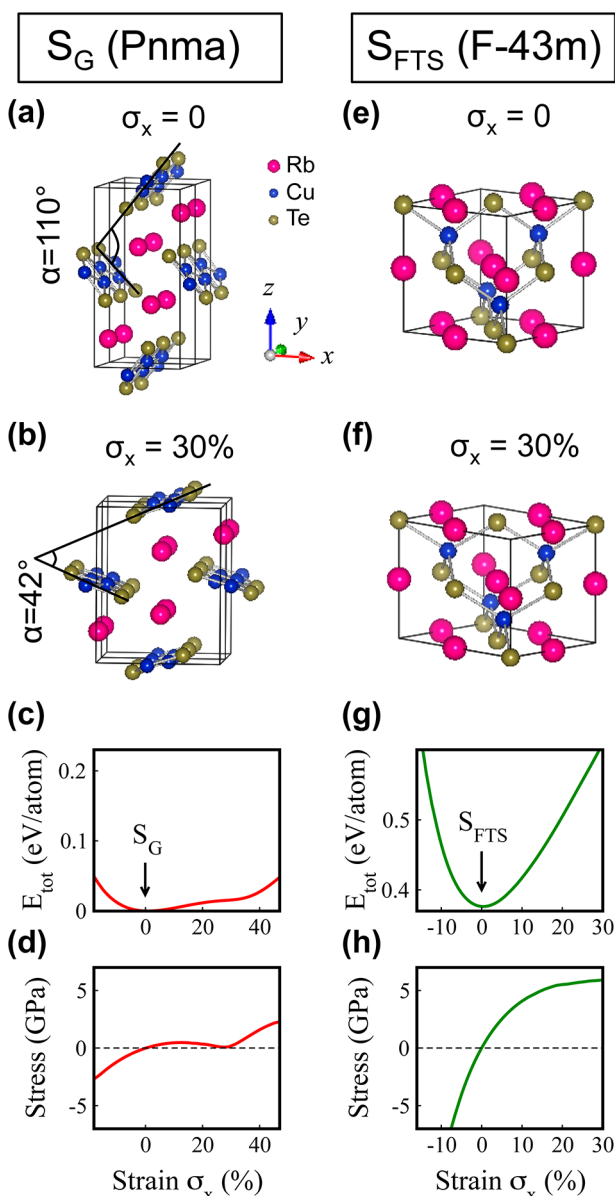


Figure 3. (a) Experimental structure (S_G) of RbCuTe without strain. (b) S_G under 30% strain along the x direction (σ_x). The angle between the plane that passes through the Te atoms in one ribbon and the plane for its nearby ribbon is denoted as α (see also α_i in Figure 2). (c) Total energy (the E_{tot} of the unstrained $Pnma$ structure is chosen as the origin) and (d) stress as functions of strain σ_x . Panels e–h are similar to panels a–d, respectively, but for RbCuTe in the filled tetrahedral structure (S_{FTS} , $F\bar{4}3m$).

matrix of elastically soft Rb atoms with channels of isolated, elastically hard 1D ribbons of $[\text{CuTe}]_{1D}$ embedded in it. Each $[\text{CuTe}]_{1D}$ ribbon is formed by four parallel Te–Cu–Cu–Te chains interconnected by Cu–Te and Cu–Cu bonds. The ribbons are arranged in ordered arrays with two types of orientations. This hybrid interdimensional structure is denoted $\text{Rb}_{3D}[\text{CuTe}]_{1D}$.

Figure 3 shows the mechanical response of $\text{Rb}_{3D}[\text{CuTe}]_{1D}$ under uniaxial strain. We start from the ground-state $Pnma$ structure S_G depicted in Figure 3a in its unstrained form where the angle between the planes of the two nano ribbons in the unit cell is $\alpha = 110^\circ$. Upon application of uniaxial strain (σ_x) along the x direction perpendicular to the $[\text{CuTe}]_{1D}$ ribbons, there is an elongation of the lattice constant a , the soft Rb matrix is deformed, and the $[\text{CuTe}]_{1D}$ ribbons rotate as shown in Figure 3b (where the angle between the planes of the two nano ribbons is now 42°) while the internal structure of the ribbons is nearly unchanged, reflecting the rigidity of $[\text{CuTe}]_{1D}$.

For strain of up to 30%, the energy increase is less than 15 meV/atom (Figure 3c), and the calculated stress (Figure 3d) is less than 0.5 GPa.⁵⁹ The fully relaxed uniaxial-strained structures (e.g., Figure 3b) are in the same structure type as the equilibrium phase (Figure 3a). In section IV of the Supporting Information, we report the result of calculations to check the stability of the orthorhombic cell (i.e., its mechanical instability) under shear strains. These calculations show that RbCuTe with $\sigma_x = 0, 30,$ and 36% is stable with respect to shear strain. Therefore, the application of uniaxial strain up to (or larger than) 30% does not cause mechanical instability in the system.⁶⁰

The very mild soft response of the hybrid interdimensional S_G structure to strain can be contrasted with the hard response of the cubic filled-tetrahedral structure (FTS; AgMgAs type, $F\bar{4}3m$) in which all atoms are interconnected [see Figure 3e with lattice constant $a = 0.714$ nm and Wyckoff positions Rb 4a (0, 0, 0), Cu 4c (1/4, 1/4, 1/4), and Te 4b (1/2, 1/2, 1/2)]. For strain up to 30% (see the strained structure in Figure 3f), the energy increases by ~ 230 meV/atom (Figure 3g), and the calculated stress (Figure 3h) is ~ 6 GPa. Furthermore, in the highly strained S_{FTS} structure, the Cu–Te zincblende-like network (Figure 3e,f) is distorted significantly and the atomic bonds in it could break causing failure of the material under large strain, producing also the large total energy increase and high stress under the strain. On the other hand, in the hybrid $\text{Rb}_{3D}[\text{CuTe}]_{1D}$ S_G , the strain changes the relative position of only the $[\text{CuTe}]_{1D}$ nano ribbons and the Rb atoms around them, keeping the tightly bonded ribbon structures unchanged. Therefore, the main structural features of RbCuTe, i.e., the $[\text{CuTe}]_{1D}$ nano ribbons and the hybrid 3D–1D structure, are robust under very large strain. Later on, we will discuss the implication of this robustness for material functionalities.

The strain tolerance of the ground-state structure of RbCuTe is the result of the 1D–3D hybrid structure of the material: strong covalent bonds (see Figure 3a) pull together the Cu and Te atoms into closed-shell rigid ribbons, whereas the Rb^+ ions forming the 3D cation network of the matrix are highly polarizable ions with outer electron clouds that are adaptable in shape. The consequence of stretching the structure along the x direction is compression along the z direction (see Figure 2) inducing a rearrangement of the Rb atoms around the rotated ribbons. The large polarizability and “softness” of the electronic cloud of the Rb cations result in a small energy cost associated with this rearrangement (“flow”) around the ribbons.

4.2. Translation of the 1D Nano Ribbon Leading to Softness in All Three Directions. The rotation of $[\text{CuTe}]_{1\text{D}}$ nano ribbons in RbCuTe (Figure 3a,b) leads to the softness in the x - z plane. However, a soft and flexible material for applications would require softness in all three directions. The softness along the y direction stems from the antiparallel shifting of the nano ribbons along the ribbon (y) axis, in light of the fact that the nano ribbons are isolated from each other by the Rb matrix and the Rb matrix is too soft to stop the ribbon from shifting.

We illustrate the simplest ribbon shifting in Figure 4, considering the relative position of the two nano ribbons in the

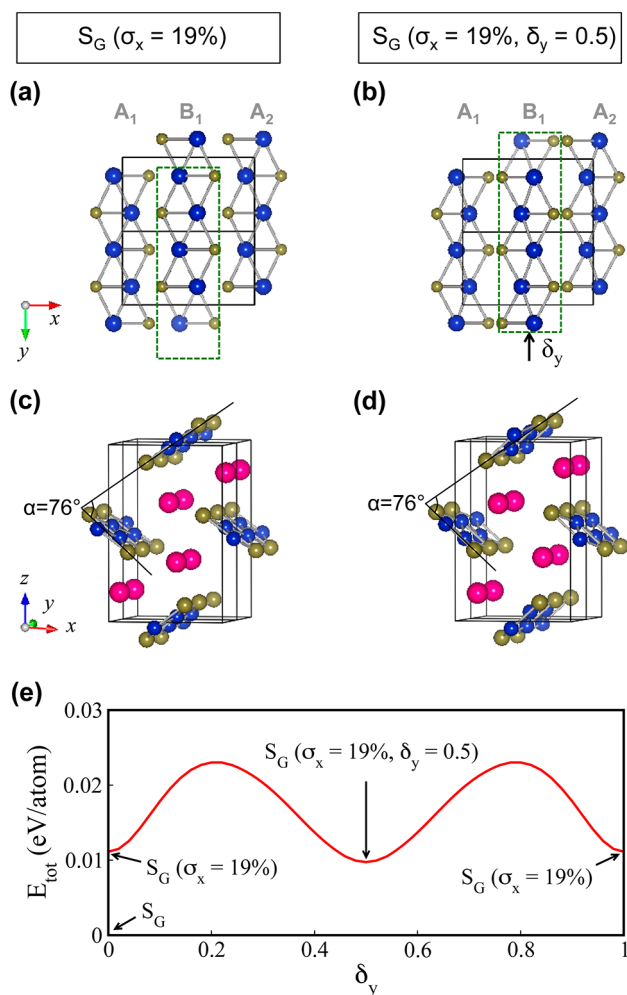


Figure 4. (a and b) Top view showing only the nano ribbons and (c and d) 3D view of the $\sigma_x = 19\%$ strained S_G structure (a and c) and the structure derived from the $\sigma_x = 19\%$ strained S_G by shifting the nano ribbon B_1 half of the lattice constant along the y direction (b and d). Along with the shifting of the B_1 ribbon, the Rb atoms change position. (e) Total energy as a function of ribbon shifting.

unit cell (A_1 and B_1 in Figure 4a,b), and shifting B_1 along the y direction continuously from 0 to the lattice constant b (on the y axis). Panels a and b of Figure 4 show the nano ribbons unshifted and shifted by $b/2$ (δ_y), and panels c and d of Figure 4 show the 3D crystal structures. We see that once the nano ribbons are shifted, the soft Rb atoms move (comparing the red spheres in Figure 4c,d) to accommodate to the new atomic environment. Surprisingly, this type of significant change of structures (approximately half of the atoms moved half of the

lattice constant) costs a total energy change of <14 meV/atom. Furthermore, the E_{tot} versus δ_y plot demonstrates two valleys at $\delta_y = 0$ and $\delta_y = 0.5$ caused by the periodic zigzag form of the $[\text{CuTe}]_{1\text{D}}$ nano ribbons (see Figure 4a,b). Therefore, the shifting of nano ribbons could be much easier than their continuous rotation as shown in panels a and b of Figure 3. The former is discrete. The discrete shifting patterns (e.g., in Figure 4b) of the $[\text{CuTe}]_{1\text{D}}$ ribbons in the $\text{Rb}_{3\text{D}}[\text{CuTe}]_{1\text{D}}$ can lead to different crystallographic forms of RbCuTe within the same hybrid 3D–1D structure family. The low transformation barrier (Figure 4e) offers the opportunity to tune the material between the polymorphs that can have very different shapes (see, e.g., Figures 3a and 4d), thus realizing functionalities utilizing controllable shapes of 3D materials. The ease of shifting $[\text{CuTe}]_{1\text{D}}$ ribbons along the y direction (Figure 4) and of their rotations in the x - z plane (Figure 3) makes the $\text{Rb}_{3\text{D}}[\text{CuTe}]_{1\text{D}}$ hybrid structures soft in all three directions.

5. ROBUST 1D ELECTRONIC STRUCTURE IN 3D MATERIALS UNDER A LARGE STRAIN

The proposed hybrid structures with a 1D nano ribbon embedded in a 3D matrix allow the outstanding softness of 3D inorganic materials. For the potential application of this general type (not necessarily only RbCuTe) of hybrid inorganic structures in flexible devices, we add a strict condition to the design principles of such materials; i.e., their material functionality should be robust under a very large strain. The robustness of inorganic flexible devices is achieved by using nano crystals that are unchanged under strain, which in turn changes only the environment between them. The hybrid structures resemble the nano crystals; however, the hybrid materials are continuous 3D crystals that could offer better performances and a simplified fabrication process.

The robustness of material functionalities under very large strain is rarely seen in inorganic materials. Panels a and b of Figure 5 show the variation of electronic structures of RbCuTe in the filled-tetrahedral structure, as an example. We see that under zero strain, RbCuTe (S_{FTS}) is a direct gap semiconductor, which, however, becomes a metal under 30% uniaxial strain. Surprisingly, for $\text{Rb}_{3\text{D}}[\text{CuTe}]_{1\text{D}}$ (S_G) (see Figure 5c,d), the same large strain (30%) leaves the band gap and overall band structure nearly unchanged. This remarkable robustness of the electronic structure under significant strain in the proposed hybrid inorganic structures extends the boundary of the strain effect in 3D inorganic crystals. In Figure S7, we show that the two crystal structures in panels a and b of Figure 4 have very similar energy bands; i.e., the shifting of the nano ribbon almost does not change the electronic structure.

We see that (Figure 5c,d) the electronic bands near the VBM in the ground-state structure of RbCuTe have a strong dispersion along the Γ - Y direction (parallel to the ribbons) but nearly zero dispersion along the Γ - X and Γ - Z directions, analogous to the one-dimensional electronic structures. To further demonstrate the 1D nature of band structure, we show the total and partial density of states of $\text{Rb}_{3\text{D}}[\text{CuTe}]_{1\text{D}}$ in Figure 6a (the density of states from HSE06⁶¹ calculations is discussed in Figure S8; the key feature of the 1D electronic structure does not change in HSE06). We find a clear step shape of density of states near VBM (Figure 6a), which is a feature of the periodic 1D electronic structures in 3D material (3D momentum space).

The calculations in this work were performed using scalar relativistic pseudopotentials neglecting spin orbit coupling

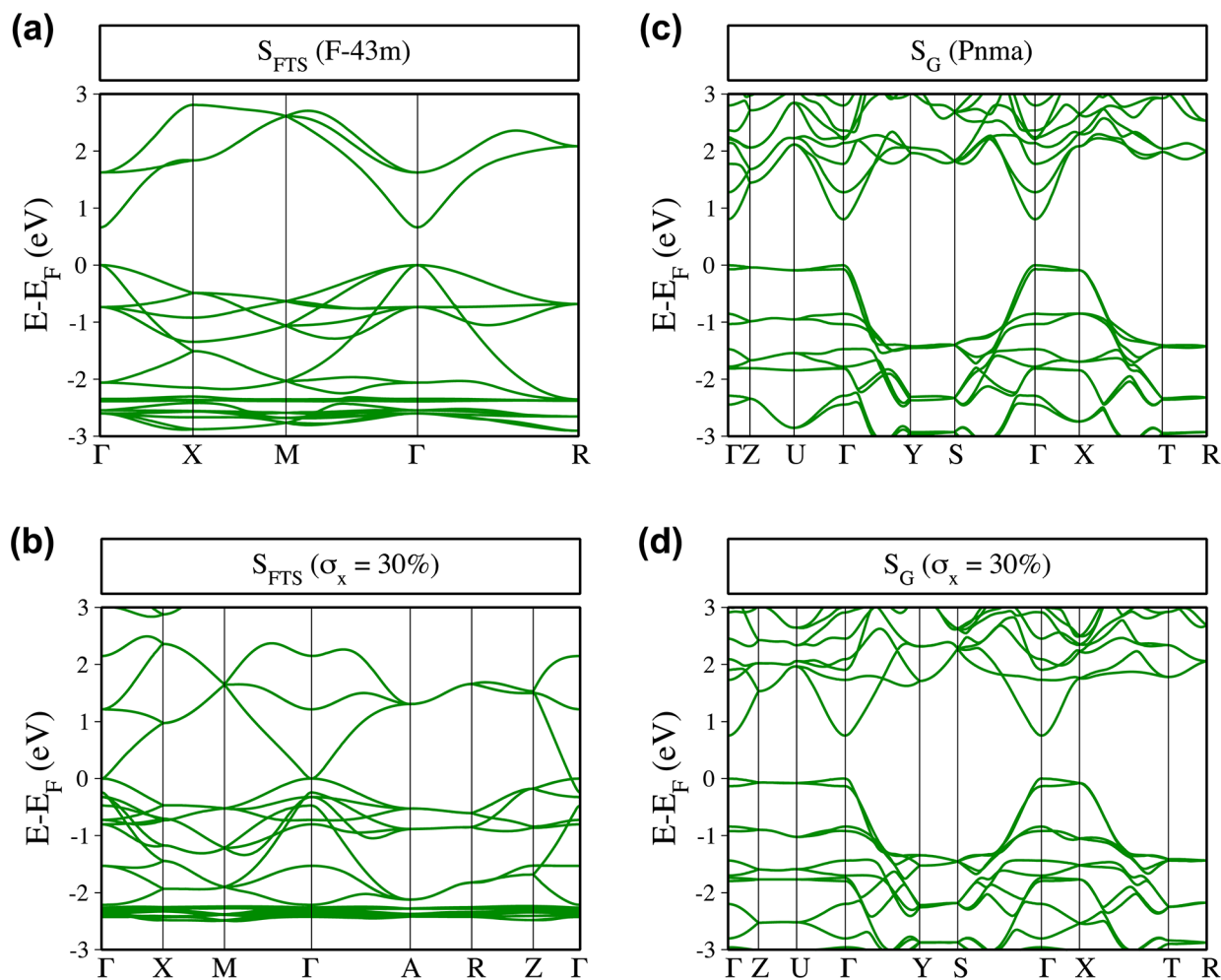


Figure 5. Band structures of RbCuTe in the S_{FTS} (a and b) and S_{G} (c and d) structures with zero (a and c) and 30% (b and d) strain σ_x .

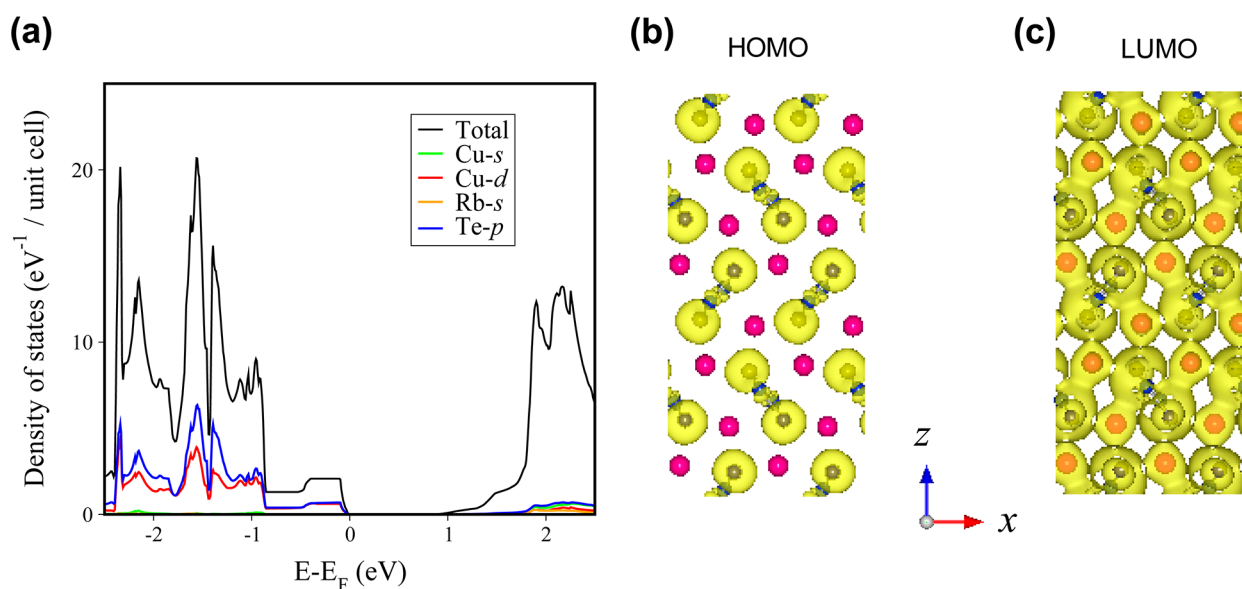


Figure 6. (a) Density of states of RbCuTe in unstrained S_{G} structure. (b and c) HOMO and LUMO wave functions squared.

(SOC). Figure S9 shows that SOC has but a negligible effect (band gap changes of ~ 15 meV) on the electronic structure near the band edges. This is so because the CBM states are mainly s-like and the VBM states are strongly hybridized Cu-d

and Te-p states, whereas the SOC effect for s-states or Cu-d states is very small.

The wave functions squared of the HOMO and LUMO states are shown in panels b and c of Figure 6. We see that the

HOMO is localized on the $[\text{CuTe}]_{1\text{D}}$ nano ribbons and the LUMO state is quite delocalized with a major contribution from $[\text{CuTe}]_{1\text{D}}$. Therefore, the electronic states near the band edges are mainly from the $[\text{CuTe}]_{1\text{D}}$ ribbons, and because the ribbons are not changed during huge structure modification (see Figures 3 and 4), the main material functionalities such as semiconducting and pseudo-1D transport similarly do not change.

6. CONCLUSIONS

This work identifies a class of simple inorganic structures that constitute a case of interdimensional hybrid structures (IDHS) and, specifically, exhibit 1D nano ribbons embedded in a 3D atomic lattice. Prediction and synthesis of a first prototype of such structures, i.e., RbCuTe , were demonstrated. Application of first-principles electronic structure calculations reveals remarkably that such structural topologies can tolerate very large strain with minimal consequences for both the 1D electronic bands and the ensuing stress. The reason is that the CuTe nano ribbons in RbCuTe can utilize their rotational degrees of freedom within the 3D atomic lattice formed by Rb , thus circumventing the fast increase in stress as a result of strain that usually characterizes conventional solids made of a contiguous set of bonds. This mechanism of rotation of 1D nano ribbons within a 3D network might offer a general “design principle” for future identification and laboratory testing of novel strain tolerant compounds. Furthermore, the combination of predictive, material-dependent theory with innovative synthesis and *in situ* characterization demonstrated here promises to establish an effective platform for discovery of materials with target functionalities.

■ ASSOCIATED CONTENT

Supporting Information

The Supporting Information is available free of charge on the ACS Publications website at DOI: 10.1021/jacs.5b06182.

Methods and results for the prediction of the crystal structures and thermodynamic stability (Figures S1–S3), comparison of results from different theoretical methods (Figures S4 and S5 as well as Tables S1 and S2), stability under shear strain (Figure S6), and additional electronic structures (Figures S7–S9) (PDF)

Crystallographic data (CIF)

■ AUTHOR INFORMATION

Corresponding Author

*alex.zunger@colorado.edu

Present Address

^{||}M.D.D.: Surface Chemistry Branch, Code 6170, Naval Research Laboratory, Washington, DC 20375, USA.

Author Contributions

[#]M.J.D.V. and X.Z. contributed equally to this work.

Notes

The authors declare no competing financial interest.

■ ACKNOWLEDGMENTS

The work of M.J.D.V., P.J.C., and K.R.P. was supported in part by the U.S. Department of Energy (DOE), Basic Energy Sciences, Office of Science, under Contract DE-AC02-06CH11357. The work of X.Z. and A.Z. was supported by Office of Science, Basic Energy Science, MSE division, via

Grant DE-FG02-13ER46959. G.T. used in this research resources of the National Energy Research Scientific Computing Center (NERSC), a DOE Office of Science User Facility supported by the Office of Science of the U.S. Department of Energy under Contract DE-AC02-05CH11231. Single-crystal X-ray data were collected at Northwestern University's Integrated Molecular Structure Education and Research Center (IMSERC) at Northwestern University, which is supported by grants from NSF-NSEC, NSF-MRSEC, the Keck Foundation, the State of Illinois, and Northwestern University. We thank Dr. Liping Yu and Dr. Yonggang Yu for helpful discussions.

■ REFERENCES

- (1) Landau, L. D.; Lifshitz, E. M. *Theory of Elasticity*; Pergamon Press: New York, 1970; Vol. 7.
- (2) Li, J.; Shan, Z.; Ma, E. *MRS Bull.* **2014**, *39*, 108.
- (3) Schlom, D. G.; Chen, L.-Q.; Fennie, C. J.; Gopalan, V.; Muller, D. A.; Pan, X.; Ramesh, R.; Uecker, R. *MRS Bull.* **2014**, *39*, 118.
- (4) Bedell, S. W.; Khakifirooz, A.; Sadana, D. K. *MRS Bull.* **2014**, *39*, 131.
- (5) Peterson, R. L.; Hobart, K. D.; Yin, H.; Kub, F. J.; Sturm, J. C. *J. Appl. Phys.* **2006**, *100*, 023537.
- (6) Estili, M.; Sakka, K.; Kawasaki, A. *Nanotechnology* **2013**, *24*, 155702.
- (7) Anthony, J. E. *Nat. Mater.* **2014**, *13*, 773.
- (8) Han, T.-H.; Lee, Y.; Choi, M.-R.; Woo, S.-H.; Bae, S.-H.; Hong, B. H.; Ahn, J.-H.; Lee, T.-W. *Nat. Photonics* **2012**, *6*, 105.
- (9) Kaltenbrunner, M.; White, M. S.; Glowacki, E. D.; Sekitani, T.; Someya, T.; Sariciftci, N. S.; Bauer, S. *Nat. Commun.* **2012**, *3*, 770.
- (10) McCulloch, I. *Nat. Mater.* **2005**, *4*, 583.
- (11) Khuong, T.-A. V.; Nuñez, J. E.; Godinez, C. E.; Garcia-Garibay, M. A. *Acc. Chem. Res.* **2006**, *39*, 413.
- (12) Cooper, A. I.; Rosseinsky, M. J. *Nat. Chem.* **2009**, *1*, 26.
- (13) Horike, S.; Shimomura, S.; Kitagawa, S. *Nat. Chem.* **2009**, *1*, 695.
- (14) Yoon, B.; Luedtke, W. D.; Barnett, R. N.; Gao, J.; Desireddy, A.; Conn, B. E.; Bigioni, T.; Landman, U. *Nat. Mater.* **2014**, *13*, 807.
- (15) Fischer, D.; Carl, W.; Glaum, H.; Hoppe, R. *Z. Anorg. Allg. Chem.* **1950**, *75*.
- (16) Mudring, A. V.; Jansen, M. *Z. Kristallogr. - New Cryst. Struct.* **2001**, *216*, 482.
- (17) Sabrowsky, H.; Vogt, P. *Z. Anorg. Allg. Chem.* **1950**, 226.
- (18) Sabrowsky, H.; Schroer, U. *Z. Naturforsch., B: Anorg. Chem., Org. Chem.* **1982**, 818.
- (19) Sabrowsky, H.; Vogt-Mertens, P.; Thimm, A. *Z. Naturforsch., B: Anorg. Chem., Org. Chem.* **1985**, 1761.
- (20) Savelsberg, G.; Schaefer, H. *Z. Naturforsch., B: Anorg. Chem., Org. Chem.* **1978**, 711.
- (21) Frueh, A. J. *J. Z. Kristallogr., Kristallgeom., Kristallphys., Kristallchem.* **1955**, 299.
- (22) Seryotkin, Y. V.; Bakakin, V. V.; Pal'yanova, G. A.; Kokh, K. A. *CrystEngComm* **2014**, *16*, 1675.
- (23) Bronger, W.; Kathage, H. U. *J. Alloys Compd.* **1992**, *184*, 87.
- (24) Sabrowsky, H.; Hippler, K.; Hitzbleck, R. D.; Sitta, S.; Thimm, A.; Vogt, P.; Wortmann, R. *Z. Naturforsch., B: J. Chem. Sci.* **1998**, *44*, 893.
- (25) Sabrowsky, H.; Thimm, A.; Vogt-Mertens, P. *Z. Naturforsch., B: Anorg. Chem., Org. Chem.* **1985**, 733.
- (26) Sabrowsky, H.; Thimm, A.; Vogt-Mertens, P. *Z. Naturforsch., B: Anorg. Chem., Org. Chem.* **1985**, 1759.
- (27) Hippler, K.; Hitzbleck, R. D.; Sitta, S.; Vogt, P.; Wortmann, R.; Sabrowsky, H. *Acta Crystallogr., Sect. C: Cryst. Struct. Commun.* **1990**, *46*, 1596.
- (28) Sabrowsky, H.; Thimm, A.; Vogt, P.; Harbrecht, B. *Z. Anorg. Allg. Chem.* **1987**, *546*, 169.
- (29) Sabrowsky, H.; Vogt, P. *Z. Anorg. Allg. Chem.* **1992**, *616*, 183.
- (30) Savelsberg, G.; Schaefer, H. *Z. Naturforsch., B: Anorg. Chem., Org. Chem.* **1978**, *33*, 370.

- (31) Frueh, A. J. J.; Czamanske, G. K.; Knight, C. Z. *Kristallogr., Kristallgeom., Kristallphys., Kristallchem.* **1957**, *108*, 389.
- (32) Savelsberg, G.; Schaefer, H. J. *Less-Common Met.* **1981**, *80*, 59.
- (33) Winter, V.; Feldbaum-Moeller, E.; Fischer, K.; Vogt, P.; Sabrowsky, H. Z. *Anorg. Allg. Chem.* **1996**, *622*, 1311.
- (34) Hippler, K.; Vogt, P.; Wortmann, R.; Sabrowsky, H. Z. *Naturforsch., B: J. Chem. Sci.* **1989**, *44*, 1607.
- (35) Bronger, W.; Bomba, C.; Sabrowsky, H. J. *Less-Common Met.* **1989**, *156*, 43.
- (36) Nuriev, I. R.; Salaev, E. Y.; Nabiev, R. N. *Izv. Akad. Nauk SSSR, Neorg. Mater.* **1983**, *19*, 1074.
- (37) Hitzbleck, R. D.; Vogt, P.; Sabrowsky, H. Z. *Naturforsch., B: J. Chem. Sci.* **1989**, *44*, 1602.
- (38) Malliakas, C. D.; Kanatzidis, M. G. *J. Am. Chem. Soc.* **2007**, *129*, 10675.
- (39) Dresselhaus, M. S.; Dresselhaus, G.; Sun, X.; Zhang, Z.; Cronin, S. B.; Koga, T. *Phys. Solid State* **1999**, *41*, 679.
- (40) Song, J.-H.; Freeman, A. J.; Bera, T. K.; Chung, I.; Kanatzidis, M. G. *Phys. Rev. B: Condens. Matter Mater. Phys.* **2009**, *79*, 245203.
- (41) Androulakis, J.; Peter, S. C.; Li, H.; Malliakas, C. D.; Peters, J. A.; Liu, Z.; Wessels, B. W.; Song, J.-H.; Jin, H.; Freeman, A. J.; Kanatzidis, M. G. *Adv. Mater.* **2011**, *23*, 4163.
- (42) Gautier, R.; Zhang, X.; Hu, L.; Yu, L.; Lin, Y.; Sunde, T. O. L.; Chon, D.; Poeppelmeier, K. R.; Zunger, A. *Nat. Chem.* **2015**, *7*, 308.
- (43) Zhang, X.; Yu, L.; Zakutayev, A.; Zunger, A. *Adv. Funct. Mater.* **2012**, *22*, 1425.
- (44) Hautier, G.; Fischer, C. C.; Jain, A.; Mueller, T.; Ceder, G. *Chem. Mater.* **2010**, *22*, 3762.
- (45) Wang, S.; Wang, Z.; Setyawan, W.; Mingo, N.; Curtarolo, S. *Phys. Rev. X* **2011**, *1*, 021012.
- (46) Meredig, B.; Agrawal, A.; Kirklín, S.; Saal, J. E.; Doak, J. W.; Thompson, A.; Zhang, K.; Choudhary, A.; Wolverton, C. *Phys. Rev. B: Condens. Matter Mater. Phys.* **2014**, *89*, 094104.
- (47) Dorhout, P. K.; Evenson, C. R. I. In *Frontiers of High Pressure Research II: Applications of High Pressure to Low-Dimensional Novel Electronic Materials*; Hochheimer, H. D., Ed.; Kluwer Academic Publishers: Dordrecht, The Netherlands, 2001; p 13.
- (48) Cody, J. A.; Mansuetto, M. F.; Chien, S.; Ibers, J. A. *Mater. Sci. Forum* **1994**, *152–153*, 35–42.
- (49) Sunshine, S. A.; Kang, D.; Ibers, J. A. *J. Am. Chem. Soc.* **1987**, *109*, 6202.
- (50) Perdew, J. P.; Ruzsinszky, A.; Csonka, G. I.; Vydrov, O. A.; Scuseria, G. E.; Constantin, L. A.; Zhou, X.; Burke, K. *Phys. Rev. Lett.* **2008**, *100*, 136406.
- (51) Dudarev, S. L.; Botton, G. A.; Savrasov, S. Y.; Humphreys, C. J.; Sutton, A. P. *Phys. Rev. B: Condens. Matter Mater. Phys.* **1998**, *57*, 1505.
- (52) Kresse, G.; Furthmüller, J. *Comput. Mater. Sci.* **1996**, *6*, 15.
- (53) Kresse, G.; Joubert, D. *Phys. Rev. B: Condens. Matter Mater. Phys.* **1999**, *59*, 1758.
- (54) Perdew, J. P.; Burke, K.; Ernzerhof, M. *Phys. Rev. Lett.* **1996**, *77*, 3865.
- (55) *SAINT*, version 7.23A; Bruker AXS Instruments Inc.: Madison, WI, 2005.
- (56) Sheldrick, G. *SADABS*; University of Göttingen: Göttingen, Germany, 1996.
- (57) Sheldrick, G. *Acta Crystallogr., Sect. A: Found. Crystallogr.* **2008**, *64*, 112.
- (58) Dolomanov, O. V.; Bourhis, L. J.; Gildea, R. J.; Howard, J. A. K.; Puschmann, H. J. *Appl. Crystallogr.* **2009**, *42*, 339.
- (59) On the basis of the GGA+U error on the *a* lattice constant (3.3% in Table 1), we estimate an error in the maximal strain of approximately $\pm 1\%$.
- (60) In the theoretical study presented here, we do not investigate the possibility that the tilting angles of the nano ribbons could be modulated along the strain direction (see Figure 3a,b) in response to the applied strain (Figure S4c).
- (61) Heyd, J.; Scuseria, G. E.; Ernzerhof, M. *J. Chem. Phys.* **2006**, *124*, 219906.